Qualitative evidence of the flexoelectric effect in a single multi-wall carbon nanotube by nanorobotic manipulation

Raya El Beainou, Jean-Yves Rauch, Sounkalo Dembele, Olivier Lehmann, Laurent Hirsinger, Michel Devel

Qualitative evidence of the flexoelectric effect in a single multi-wall carbon nanotube by nanorobotic manipulation

R. El Beainou,* J-Y. Rauch, S. Dembélé, O. Lehmann, L. Hirsinger, M. Devel

FEMTO-ST Institute, Univ. Bourgogne Franche-Comté, CNRS,
ENSMM, 26 rue de l'Epitaphe, CS 51813, 25030 Besançon CEDEX, France

*Corresponding author: raya.elbeainou@femto-st.fr

Abstract

The flexoelectric effect corresponds to the linear variation of the electric polarization of a material subjected to a strain gradient (i.e. during its mechanical bending). Unlike piezoelectricity, it also exists in non-centrosymmetric materials. Furthermore, due to the gradient term, its magnitude can increase as the size of the system decreases. Thanks to this effect, nanoscale systems could be used to harvest thermal vibration energy to power a microdevice. These could be multi-wall carbon nanotubes since they are known to bend easily in an elastic manner. However, it is very challenging to experimentally measure the flexoelectric behavior of a single multi-wall carbon nanotube due to its small size (less than 50 nm in diameter), to the low level of induced charges and to the need to vary the imposed stress. To progress in this direction, a six-degree-of-freedom robot with a fiber tip is used inside a dual-beam microscope to pick up a few single carbon nanotubes from a tangle and connect them to the fiber tip. After ion-soldering the two tips, each carbon nanotube is dynamically bent several times while monitoring the brightness of the bending area and its effective radius of curvature. This allowed us to demonstrate qualitatively the flexoelectric effect at the level of a single MWCNT.

Keywords:

Flexoelectricity, nanomanipulation, carbon nanotubes, energy harvesting, polarization.

Flexoelectricity, as reviewed in [1], is the linear coupling between electrical polarization and strain gradient, predicted by Mashkevich and Tolpygo [1], and later phenomenologically described by Kogan [2]. It can now be associated to the origin of peculiar features identified as being due to non-homogeneous strain by Scott in previously measured infra-red spectra [3], while Bursian and Zaikovskii measured the converse effect at the same time [4]. However, this was rarely considered for electromechanical transduction in solids due to its small relative magnitude in macroscopic solids. Hence, this field of research was pretty inactive until Ma and Cross [5-6] got results significantly higher than expected according to the theory, after Fousek et al [7] proposed, that flexoelectric effect could be used to get an effective piezoelectric effect by vertically compressing an asymmetrically shaped material. Then, Gruverman et al. [8] showed that it was possible to change the direction of polarization on PZT capacitors by bending the substrate of silicon. Han et al [9] showed that they obtained a nanogenerator by growing PZT directly on multi-wall carbon nanotube. Other authors (e.g. [10]) developed a nanocomposite using non-homogeneous strains to obtain a behavior similar to a piezoelectric material. All these recent studies extend the potential of the flexoelectric effect.

The microscopic origin of flexoelectricity in ionic crystals can be attributed to the fact that, even in a centrosymmetric crystal (hence, one that cannot be piezoelectric), an inhomogeneous strain separates the centers of positive and negative charges and consequently induces a polarization [5]. More generally, the 4^{th} order tensor characterizing this effect, quantifies the ability of a dielectric material to polarize electrically under a strain gradient. The fact that high strain gradients can be obtained more easily at the nanoscale than at the macroscopic scale opens up possibilities for taking advantage of flexoelectricity in nanoscale systems. However, there is still no experimental report about the flexoelectricity of a single object at the nanoscale. A previous experimental study of the flexoelectric effect using thin films of Multi-Wall Carbon Nanotubes (or MWCNTs) bearing PZT microparticles [9] showed that it was possible to produce a peak output voltage of 8.6 V and an output current of 47 nA when a force of 20 N was applied. This prompted us to study this effect at the level of a single MWCNT. However, for single MWCNT manipulation and characterization, specific setups are required.

In the past years, Atomic Force Microscopy (or AFM) has appeared as a powerful and versatile tool for the characterization of nanomaterials in nanoscience and nanotechnology [11-13]. Recently, Xiao Hu et al. [14] used an AFM for MWCNT characterization in order to fabricate conical structure on a commercial conductive AFM probe with a single nanotube

protruding from its end. However, a robotic platform inside a Scanning Electron Microscope (or SEM) seems to be a more versatile tool than AFM for nano-manipulation due to the magnification from x400 to over x100.000. Indeed, this kind of platform -with dual beam SEM/ Focused Ion Beam (or FIB) - enables its users to achieve, in an original way, nanomanipulation tasks offering disruptive characterization and nanofabrication potentials: characterization of nanowires [15-17] and graphene membranes [18], assembly of photonic crystal device [19] and nano-wire based transistors [20], detailed study of DNA [21], assembly of the smallest microhouse in the world at the tip of an optical fiber [15], the smallest camera operator [22] and many others. Thus, this approach has shown great interest compared to other techniques, offering a platform with great versatility and with ease of reconfiguration and adaptation to different environments [23-26].

In this article, the flexoelectric response of some isolated MWCNTs is studied using a robotic approach, that is to say, the MWCNTs are bent in vacuum by micromanipulators, and observed using a Focused Ion Beam and a Scanning Electronic Microscope. MWCNTs are chosen because they can be reversibly bent, with a small radius of curvature, without breaking. In addition, they can have good thermal and electrical conductivity [27-29], low threshold voltage for field emission [30-32], and high mechanical strength [33,34]. In a second paragraph, our experimental setup is described. The way in which the raw data was processed is then presented and finally the results obtained are discussed.

Different types of MWCNTs are deposited on a (100) Si substrate by chemical vapor deposition (CVD) based on heptane and acetylene as a catalyst. A SMF 128 optical fiber is used in order to manipulate the MWCNTs. The optical fiber is stretched in order to have a tip diameter less than 100 nm. The purpose is to be able to use an optical fiber as a support in order to weld the MWCNT to it. Silica optical fibers allow to have a high mobility and flexibility of handling at this scale without having the disadvantages of a 5 nm to 30 nm tungsten tip, which deforms plastically on contact.

The manipulations are carried out in μRobotex station [15]. It is based on an Auriga 60 microscope from Zeiss and comprises a Scanning Electron Microscopy (SEM) column, a Focused Ion Beam (FIB) column, a Gas Injection System (GIS) and two robotic arms (a 5-degree-of-freedom stage, and a 6-degree-of-freedom robot). The FIB column is positioned at an angle of 54° from the z-axis of the SEM column. The robot consists of six stick/slip actuators

from SmartAct. A homemade real-time controller synchronizes the movement of the actuators in velocity and acceleration every 500 µs, leading to high precision positioning of the tool center of the robotic arm with an accuracy of the order of 10 nm. The control is carried out from a human-machine interface (HMI) and can be performed either in the robot frame, the SEM frame or the FIB frame.

The SEM is used to visualize the surface during electron beam welding of the MWCNT. The FIB can be used for etching, cutting, folding and imaging. The GIS air system can use three gases -platinum, carbon, xenon fluoride- and is used to deposit a thin layer of naphthalene onto the tip of the previously metallized optical fiber, which helped fix the MWCNT afterwards [35]. The optical fiber has an inclination of 54° with respect to the vertical axis -z axis of FIB-, in order to be in the intersection of the focal planes of SEM and FIB (see Figure 1).

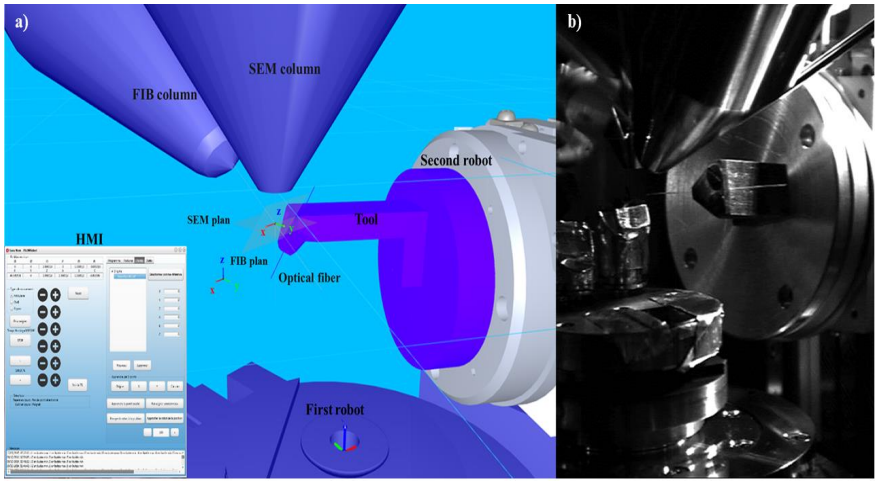

Figure 1: a) CAD representation of vacuum chamber interior showing SEM, FIB, first and second robot (with the tool carrying the optical fiber) and a screen copy of the human machine interface (HMI) b) Photo of the same chamber

The manipulation procedure starts with the search for an isolated MWCNT in the MWCNT tangle, the free end of which is then welded to the thin naphthalene layer covering the tip of the metallized optical fiber. A low current of 1 pA is used in order to avoid damaging both the tip and the MWCNT. After extraction of the MWCNT from the tangle, its new free end is welded on a grounded Si substrate (Figures 2a and 2b). This MWCNT is subjected to repetitive local bending by repeated horizontal translations of the optical fiber. Then, a variation of the brightness of the bent part is observed as the local curvature radius of the MWCNT

changes over time (Figures 2c, 2d and 2e). This effect is mainly attributed to a local variation in bound surface electric charges that appear due to the flexoelectric effect, as detailed in the next section. In order to study this effect, the apparent radius of curvature in the plane of observation is measured by first defining a square region of interest (ROI) containing the bent part. Then, before the nanotube is bent, the maximum level of brightness, in the ROI, is determined. The pixels with a positive variation of brightness when the nanotube is bent, are then used to fit a circle, which radius determines the apparent radius of curvature in the observation plane. This radius could also be estimated using the ImageJ software, by drawing an osculating circle tangent to the bent part and measuring its radius. This procedure is repeated ten times in order to average the errors (e.g. due to the operator). The standard deviations for these measures vary between 0.007 and 0.048 µm.

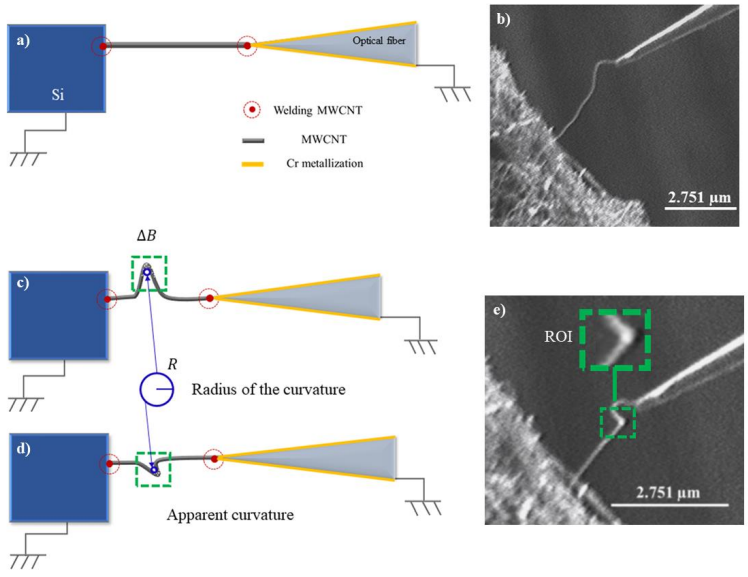

Figure 2 a) Schematic representation of the setup: a MWCNT is welded on the tip of an optical fiber and on a Si cantilever. b) FIB observation of that setup. c) and d) schemes of the bent MWCNT after translation of the Si cantilever. e) FIB observation of the bent MWCNT. The green square defines the region of interest (ROI) used to measure the apparent radius of curvature.

Generally, there is an accumulation of free electric charges at sharp ends of conductors (tip effect). These electric charges create a local electric field that interacts with an incident beam of charged particles (i.e. electrons in the case of an SEM imaging and Gallium ions in the

case of a FIB imaging), which can result in an increase of secondary electrons. Seen through an electron detector, these areas appear brighter than the other areas. As MWCNTs can have both semiconducting and metallic walls, this could be the explanation of the increase of brightness that we see in the bent parts. However, we have checked that, in our case, the outer parts of the MWCNTs we used, are electrically insulating enough so that they do not show a tip effect. This can be seen in the SEM image presented in Figure 3, where the nanotube tip on the left (area A) presents no relative increase of brightness but an almost uniform grey level (with a slight shading effect revealing that the incident beam of particles arrives from above the image on the left). However, in this same figure (i.e. with the same settings) one can see that the brightest areas correspond to the most strongly curved and best oriented areas with respect to the incident beam (see areas B and C). We tentatively attribute this local increase of brightness to the presence of bound (and not free) electric charges that are induced by the flexoelectric effect as explained below.

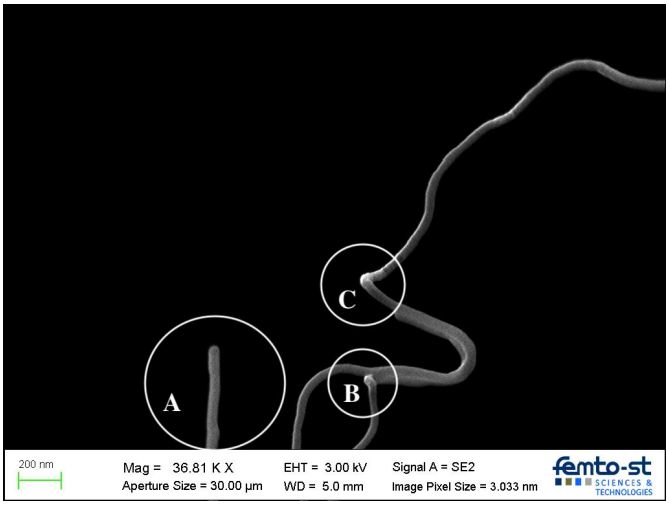

Figure 3) SEM observation of MWCNTs: tip of a single nanotube (area A on the left) and more or less strongly curved nanotubes (areas B and C on the right).

In a continuous medium model, the flexoelectric effect can be expressed as an additional term to piezoelectricity in the constitutive equation of the polarization of a material subjected to an external electric field and mechanical strain:

$$P_i = \varepsilon_0 \chi_{ij} E_j + e_{ijk} S_{jk} + \mu_{ijkl} \frac{\partial S_{jk}}{\partial x_l} \quad (1)$$

where i, j, k are indices denoting directions (in $\{x, y, z\}$), P is the polarization vector, χ the dielectric susceptibility tensor, e the piezoelectricity tensor, S the symmetrized strain tensor, μ the 4th order flexoelectricity tensor, and $\partial S_{jk}/\partial X_l$ the strain gradient tensor. For a thin membrane, this gradient corresponds to the mean curvature $2\,C = (1/R_{min} + 1/R_{max})$ where R_{min} and R_{max} are the principal radii of curvature. Therefore, in a non-piezoelectric material such as MWCNTs, the polarization $\vec{P}_c$ due to its curvature, in the radial direction is such that:

$$\left\|\vec{P}_c\right\| = 2\,\mu_{eff}\,C \tag{2}$$

where μ_{eff} denotes the effective flexoelectric coefficient, that can be evaluated using an atomic-scale effective flexoelectric coefficient $F = 0.831$ D.Å = 0.173 e.Å^2/atom computed by Kvashnin et al. [37] using Density Functional Theory (in good agreement with results between 0.157 e.Å^2/atom et 0.187 e.Å^2/atom, depending on the structure, obtained by Kalinin and Meunier [38], also using DFT), which gives $\mu_{eff} = F/V_{at} = 0.173 \cdot 1.6 \cdot 10^{-19} \cdot 10^{-20}/\left(\left(3\sqrt{3} \cdot (1.42 \cdot 10^{-10})^2/4\right) \cdot 0.8 \cdot 10^{-10}\right) = 1.32 \cdot 10^{-10}$ C/m, using the thickness estimate of Kalinin and Meunier [38] to compute the volume per atom (V_{at}). We note that this value is in good agreement with the macroscopic order of magnitude (10^{-10} C/m) estimated by Kogan [39] for crystalline materials.

Since a nanotube corresponds to a graphene sheet folded into a cylinder of radius r_0, we have a mean curvature $2\,C_0 = 1/r_0$. When this nanotube is bent with a mean radius R, we have a mean curvature, for points inside the bend, $2\,C_{in} = (1/r_0 - 1/(R - r_0))$, and, for points outside the bend, $2\,C_{out} = (1/r_0 + 1/(R + r_0))$ [36]. Therefore, the macroscopic variation of polarization due to curvature $\Delta\vec{P}_{c,o}$ between points outside the bend and points in the straight part of the nanotube is such that

$$\left\|\Delta\vec{P}_{c,o}\right\| = 2\,\mu_{eff}\,(C_{out} - C_0) = \frac{\mu_{eff}}{R + r_0} \tag{3}$$

Similarly, $\Delta\vec{P}_{c,i} = \mu_{eff}/(R - r_0)$ between points inside the bend and points in the straight part of the nanotube These macroscopic variations of polarization $\Delta\vec{P}_{c,o}$ and $\Delta\vec{P}_{c,i}$ (coming from the outward atomic dipoles created by the flexoelectric effect) can also be modelled by variations in the surface densities of bound electric charge $\Delta\sigma$ such that (with $\vec{n}$ the unit vector normal to the surface from the center of curvature):

$$\Delta\vec{P}_c \cdot \vec{n} = \Delta\sigma \tag{4}$$

which is not exactly the same for the parts of the outer surface of the bent MWCNT that are inside and outside of the bend, since their radii of curvature are not exactly the same. For a typical curvature of 30 μm^{-1}, we can use our estimate of μ_{eff} to compute a corresponding variation of surface charge density of $1.32 \cdot 10^{-10} \cdot 3 \cdot 10^{7} = 4 \cdot 10^{-3}$ C.m^{-2}. This variation of bound electric charge creates a local electric field which, if sufficiently intense, can induce a detectable increase of brightness in this bent area in the SEM and FIB images. For the sake of simplicity, a linear relationship between the change in brightness ΔB and the change in bound electric charge is tentatively assumed:

$$\Delta B \propto \Delta\sigma \approx \frac{\mu_{eff}}{R} \quad (4)$$

This implies that the local change of brightness, caused by the bending, would be inversely proportional to its mean bending radius R, which can be validated (or not) by recording images of the MWCNT as it is bent.

As described in the previous section, the flexoelectric response of isolated MWCNTs is explored by manipulating them within our SEM-FIB-based microrobotic system [16]. Figure 4 presents FIB observations of a tangle of MWCNTs during its bending. Image 4a shows some brightness points on different MWCNTs deposited on the Si substrate. These MWCNTs are very flexible and tend to orient following the field of the FIB. One side of a MWCNT is attached on the tip of the optical fiber and extracted from the tangle of MWCNTs. Image 4b shows the same MWCNT bent as a result of translating the optical fiber. The MWCNT has a diameter between 15 nm and 20 nm. The FIB observations in images 4b 4c and 4d show that the bending location appears with a brighter white color than the surrounding parts of the MWCNT. One can clearly see that the more it is bent, the brighter it appears, thus demonstrating qualitatively the flexoelectric effect.

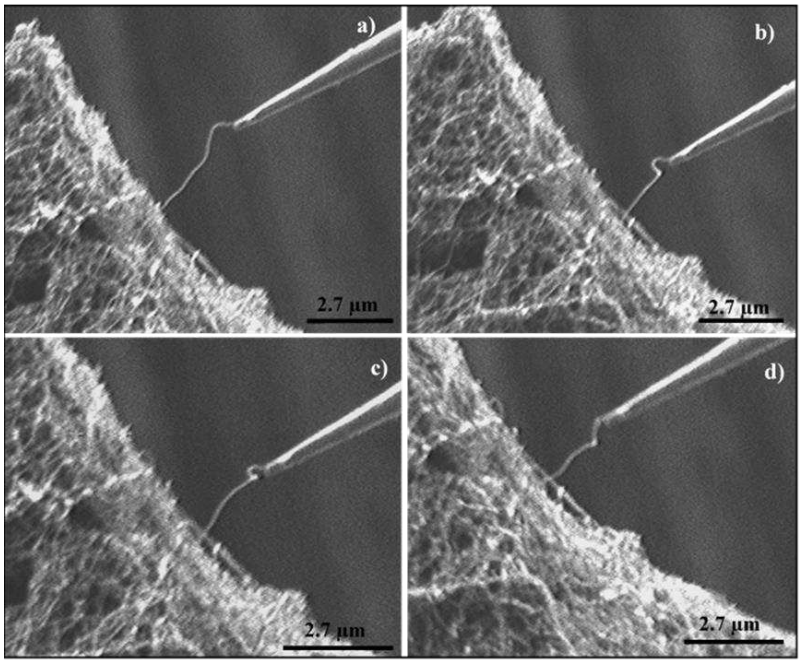

Figure 4 FIB observations of MWCNTs deposited with CVD. a) A single 20 nm diameter MWCNT extended by the tip of an optical fiber. b), c), d) the same MWCNT bent three times.

In order to be more quantitative, computer vision tools are used to analyze the bending region in the successive images and to extract both the brightness variations in this region and the apparent radius of curvature. The variation of the brightness ΔB in the ROI, as a function of the index of the image in the recorded movie, is represented in Figure 5.

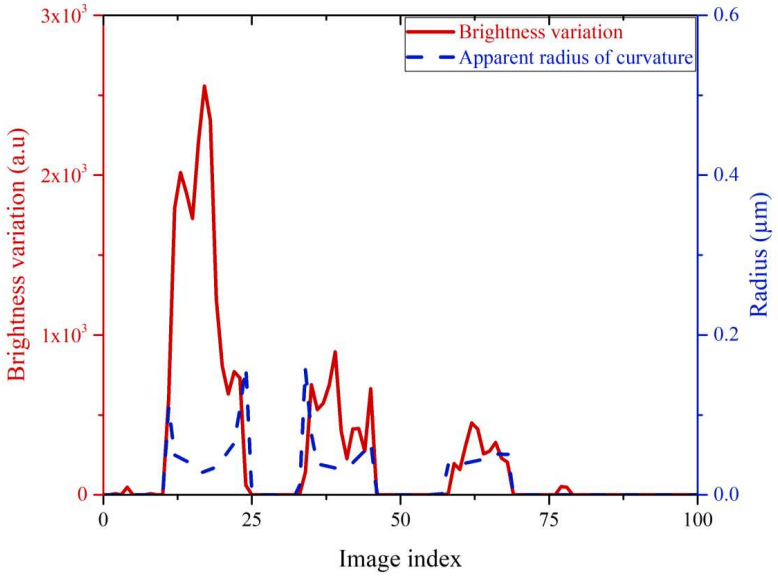

Figure 5: Variation of brightness (solid curve) and apparent radius of curvature (dashed curve) in the region of bending with respect to the index of the image in the sequence of images. Peaks of brightness variation correspond to maximum of bending.

On the whole, Figure 5 shows three peaks of brightness variations corresponding to three different translations of the tip fiber, held by the robot, and three radii of curvature. In addition, various phenomena related to electric charges, such as image drift or aberrations in the formation of the image were observed in FIB images. Furthermore, it is highly probable that the bending of the MWCNT is not in the plane of observation of the FIB therefore introducing a projection error. The fact that the MWCNT does not bend in a single plane (as can be easily seen by manipulating, for example, a shoelace) complicates the interpretation. Nevertheless, Figure 6 shows a good correlation between the brightness variations for each peak and the apparent curvature $1/R$, thus confirming our qualitative interpretation by a flexoelectric effect.

A more quantitative determination of the effective flexoelectricity coefficient requires a method to compute the changes of local electric charge from the brightness variations. We have been trying to measure the current that can be produced by the repeated bending of a MWCNT, with a nano-ammeter electrode located close to the tip of that MWCNT, but up to now the values obtained are still too noisy to be used.

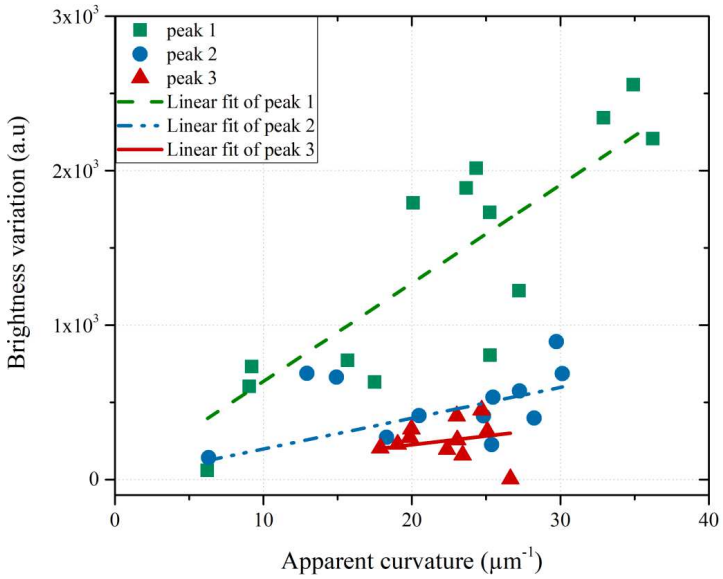

Figure 6: Brightness variation ΔB as a function of the apparent curvature (μm^{-1}) for the three peaks.

Very challenging manipulations of MWCNTs are performed in secondary vacuum, in order to repeatedly bend a single MWCNT in the common focal plane of a SEM and a FIB. A region of interest is selected around the bent part of the MWCNT in order to measure the local variations of brightness in that region, and correlate them with variations of its apparent radius of curvature. Since these variations of brightness can be attributed to variations of local electric charge such as those due to the polarization of the MWCNT as a result of the imposed strain gradient, the observation of, approximatively linear variations of brightness as a function of the apparent radius of curvature during the bending of a single MWCNT qualitatively reveals its flexoelectric response.

Acknowledgements

This work was supported by the EIPHI Graduate School (contract "ANR-17-EURE-0002"), the Region of Bourgogne Franche-Comté, the French RENATECH network and the Equipex ROBOTEX project (contract ANR-10-EQPX-44-01). We thank Mohammad Arab Pour Yazdi and Thierry Barriere for the MWCNT samples deposited on silicon substrate.

Data availability

The data that support the findings of this study are available from the corresponding author upon reasonable request.

References

[1] V. S. Mashkevich and K. B. Tolpygo, "Electrical, optical and elastic properties of diamond crystals" Soviet Physics JETP, 5(3), 435-439 (1957).

[2] S. Kogan, "Piezoelectric effect during inhomogeneous deformation and acoustic scattering of carriers in crystals," Sov. Phys. Solid State., 5, 10, 2069–70, (1964).

[3] J. F. Scott, "Lattice Perturbations in $CaWO_4$ and $CaMoO_4$", J. Chem. Phys., 48, 874-876 (1968)

[4] E. V. Bursian and O. I. Zaikovskii, "Changes in the curvature of a ferroelectric film due to polarization", Sov. Phys.–Solid State, 10 (5), 1121-1124 (1968)

[5] W. Ma and L. E. Cross, "Large flexoelectric polarization in ceramic lead magnesium niobate," Appl. Phys. Lett., 79 (26) 4420–4422 (2001)

[6]W. Ma and L. E. Cross, "Observation of the flexoelectric effect in relaxor $Pb(Mg_{1/3}Nb_{2/3})O_3$ ceramics," Appl. Phys. Lett.,78, 19, 2920–2921 (2001)

[7] J. Fousek, L. E. Cross, D. B. Litvin, "Possible piezoelectric composites based on the flexoelectric effect," Mater. Lett., 39, 5, 287–291 (1999)

[8] A. Gruverman, B. J. Rodriguez, A. I. Kingon, R. J. Nemanich., "Mechanical stress effect on imprint behavior of integrated ferroelectric capacitors," Appl. Phys. Lett., 83 (4), 728–730 (2003)

[9] J. K. Han, D. H. Jeon, S. Y. Cho, S.W. Kang, S. A. Yang, S. Don Bu, S. Myung, J. Lim, Moonkang Choi, M. Lee, M. Ku Lee, "Nanogenerators consisting of direct-grown piezoelectrics on multi-walled carbon nanotubes using flexoelectric effects," Sci. Rep., 6 (1), 29562 (2016)

[10] B. Chu, W. Zhu, N. Li, L. E. Cross, "Flexure mode flexoelectric piezoelectric composites," J. of Appl. Phys., 106 (10), 104109 (2009)

[11] H. J. Butt, B. Cappella and M. Kappl, "Force measurements with the atomic force microscope: Technique, interpretation and applications", Surf. Sci. Rep., 59, 1–152 (2005)

[12] R. Garcia and R. Perez, "Dynamic atomic force microscopy methods" Surf. Sci. Rep., 47, 197–301 (2002)

[13] F. J. Giessibl, "Advances in atomic force microscopy" Rev. Mod. Phys., 75, 949–983 (2003)

[14] X. Hu, H. Wei, Y. Deng, X. Chi, J. Liu, J. Yue, Z. Peng, J. Cai, P. Jiang, L. Sun, "Amplitude response of conical multiwalled carbon nanotube probes for atomic force microscopy", RSC Adv., 9, 429–434 (2019)

[15] J.-Y. Rauch, O. Lehmann, P. Rougeot, J. Abadie, J. Agnus, and Miguel. A. Suarez, "Smallest microhouse in the world, assembled on the facet of an optical fiber by origami and welded in the μRobotex nanofactory," J. Vac. Sci. Technol. A, 36 (4), 041601 (2018)

[16] A. Lugstein, M. Steinmair, A. Steiger et al. "Anomalous piezoresistance effect in ultrastrained silicon nanowires", Nano Letters, 10, 3204–3208 (2010)

[17] Y. Zhu, Q. Qin, F. Xu, F. Fan, Y. Ding, T. Zhang, B. J. Wiley, Z. Lin Wang, "Size effects on elasticity, yielding, and fracture of silver nanowires: In situ experiments". Phys. Rev. B, 85, 045443 (2012)

[18] S. Zimmermann, T. Tiemerding, S. Fatikow, "Automated robotic manipulation of individual colloidal particles using vision-based control". IEEE/ASME Transactions on Mechatronics, 20 (5), 2031–2038 (2015)

[19] K. Aoki, H.T. Miyazaki, H. Hirayama, K. Inoshita, T. Baba, K. Sakoda, N. Shinya Y. Aoyagi, "Microassembly of semiconductor threedimensional photonic crystals". Nature Materials, 2, 117–121, (2003)

[20] Y.L. Zhang, J. Li, S. To, Y. Zhang, X. Ye, L. You Yu Sun, "Automated nanomanipulation for nanodevice construction," Nanotechnology, 23, 065304 (2012)

[21] B. K. Chen, D. Anchel, Z. Gong, R. Cotton, R. Li, Y. Sun, and D. P Bazett-Jones, "Nano-dissection and sequencing of DNA at single sub-nuclear structures". Small, 10, 3267–3274 (2014)

[22] O. Lehmann, J.-Y. Rauch, Y. Vitry, T. Pinsard, P. Lambert, M. Gauthier, "Miniaturized robotics, the smallest camera operator bot pays tribute to David Bowie", IEEE Robotics & Automation Magazine, 27 (3), 22-28 (2020)

[23] C. Ru, Y. Zhang, Y. Sun, D Hoyle, I. Cotton. "Automated four-point probe measurement of nanowires inside a scanning electron microscope". IEEE Transactions on Nanotechnology, 10, 674–681 (2011)

[24] Y. Zhang, XY. Liu, CH. Ru; J. Luo; S. Xie, and Y. Sun, "Automated pick-place of silicon nanowires". IEEE Transactions on Automation Science and Engineering, 10, 554–561, (2013)

[25] Y. Zhang, X. Liu, C. Ru; Y. Liang Zhang; L. Dong; Y. Sun "Piezoresistivity Characterization of synthetic silicon nanowires using a MEMS device". Journal of Microelectromechanical Systems, 20, 959–967 (2011)

[26] H. Xie, S. Régnier, "High-efficiency automated nanomanipulation with parallel imaging/manipulation force microscopy". IEEE Transactions on Nanotechnology, 11 (1), 21-33 (2012)

[27] F. Du, J. E. Fischer, K. I. Winey, "Effect of nanotube alignment on percolation conductivity in carbon nanotube/polymer composites," Phys. Rev. B, 72 (12), 121404, (2005)

[28] H. R. Astorga and D. Mendoza, "Electrical conductivity of multiwall carbon nanotubes thin films," Opt. Mater., 27 (7), 1228–1230 (2005)

[29] R. Haggenmueller, C. Guthy, J. R. Lukes, J. E. Fischer, and K. I. Winey, "Single wall carbon nanotube/polyethylene nanocomposites: Thermal and electrical conductivity," Macromol., 40 (7), 2417–2421 (2007)

[30] A. G. Umnov, T. Matsushita, M. Endo, and Y. Takeuchi, "Field emission from flexible arrays of carbon nanotubes," Chem. Phys. Lett., 356 (3–4), 391–397 (2002)

[31] C. Y. Wang, T. H. Chen, S. C. Chang, T. S. Chin, and S. Y. Cheng, "Flexible field emitter made of carbon nanotubes microwave welded onto polymer substrates," Appl. Phys. Lett., 90 (10), 103111 (2007).

[32] P. Hojati-Talemi, S. C. Hawkins, C. P. Huynh, and G. P. Simon, "Highly efficient low voltage electron emission from directly spinnable carbon nanotube webs," Carbon, 57, 169–173 (2013)

[33] T. Ramanathan, H. Liu, L. C. Brinson, "Functionalized SWNT/polymer nanocomposites for dramatic property improvement," J. Polym. Sci. B Polym. Phys., 43 (17), 2269–2279 (2005)

[34] S. D. McCullen, D. R. Stevens, W. A. Roberts, S. S. Ojha, L. I. Clarke, and R. E. Gorga, "Morphological, electrical, and mechanical characterization of electrospun nanofiber mats containing multiwalled carbon nanotubes," Macromol., 40 (4), 997–1003 (2007)

[35] G. Calafiore, A. Koshelev, T. P. Darlington, N. J. Borys, M. Melli, A. Polyakov, G. Cantarella, F. I. Allen, P. Lum, E. Wong, S. Sassolini, A. Weber-Bargioni, P. J. Schuck, S. Cabrini, and K. Munechika, "Campanile Near-Field Probes Fabricated by Nanoimprint Lithography on the Facet of an Optical Fiber," Sci. Rep.,7 (1), 1651 (2017)

[36] T. D. Nguyen, S. Mao, Y.-W. Yeh, P. K. Purohit, M. C. McAlpine, "Nanoscale Flexoelectricity", Adv. Mater., 25 (7), 946-974, (2013).

[37] A. G. Kvashnin, P. B. Sorokin, B. I. Yakobson, "Flexoelectricity in carbon nanostructures: Nanotubes, Fullerenes, and Nanocones", J. Phys. Chem. Lett., 6 (14), 2740-2744 (2015)

[38] S. V. Kalinin, V. Meunier, "Electronic flexoelectricity in low-dimensional systems", Phys. Rev. B, 77(3), 033403 (2008)

[39] S. M. Kogan, "Piezoelectric effect during inhomogeneous deformation and acoustic scattering of carriers in crystal", Sov. Phys. Solid State 5(10), 2069-2070 (1964) (or Fiz. Tverd. Tela (Leningrad) 5, 2829 (1963))

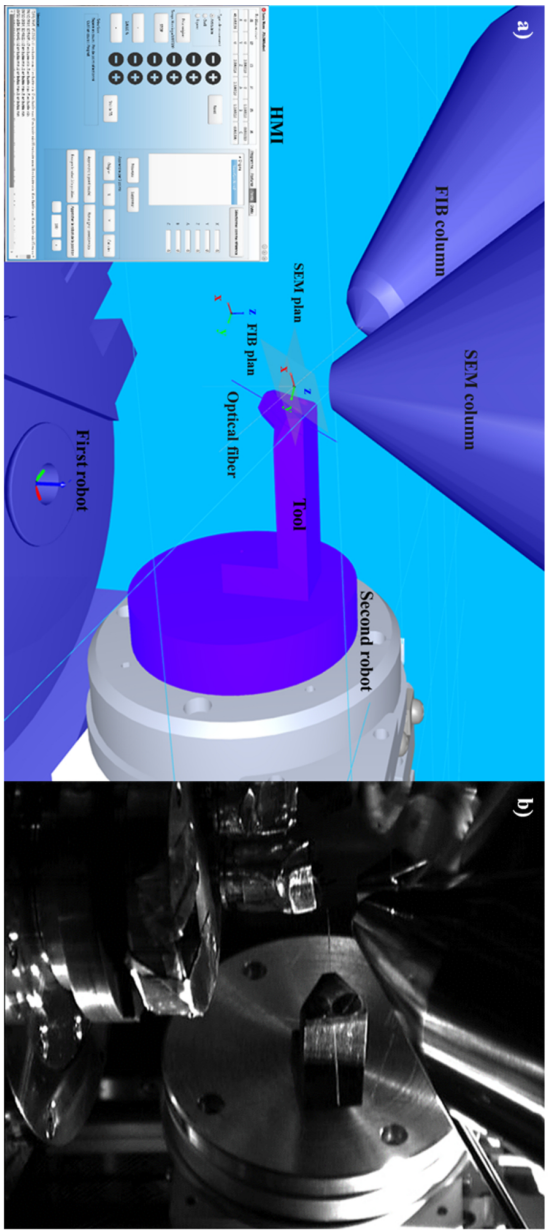

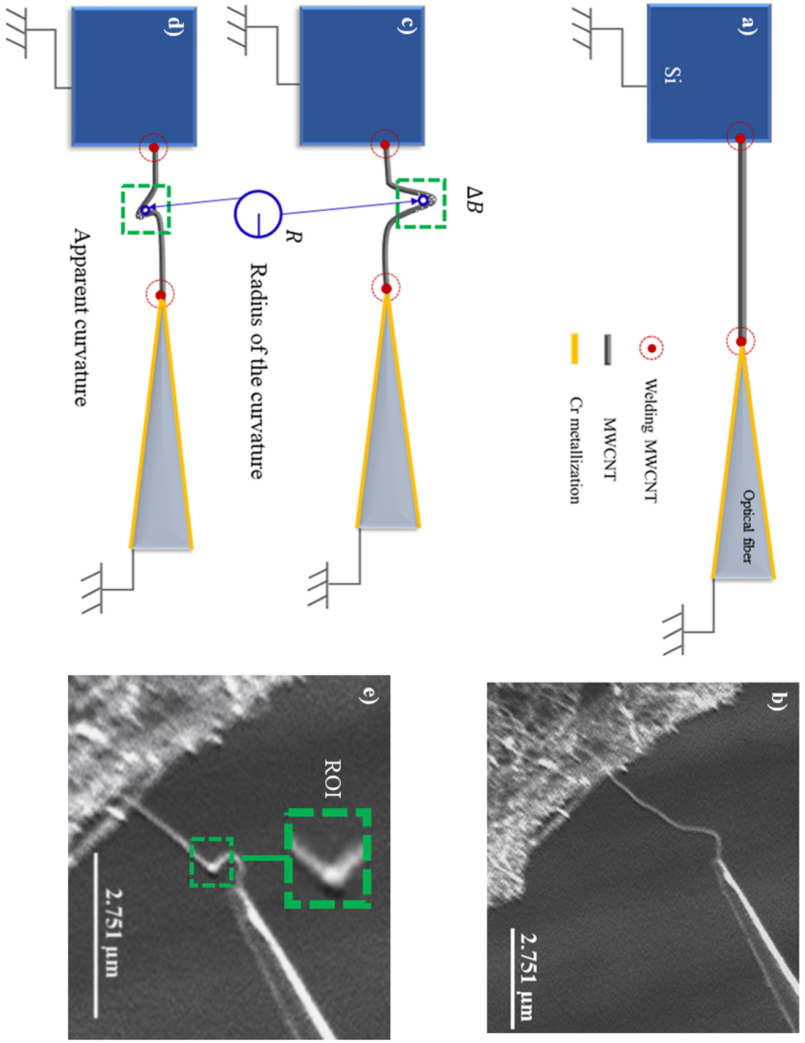

PLEASE CITE THIS ARTICLE AS DOI: 10.1063/5.0065214

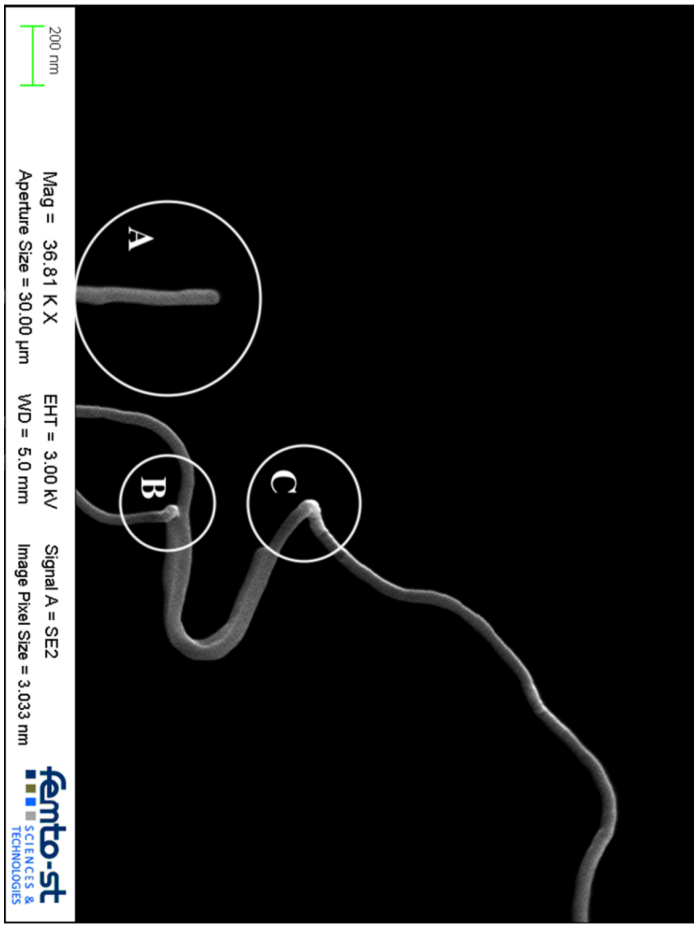

PLEASE CITE THIS ARTICLE AS DOI: 10.1063/5.0065214